Control of Ramp-Up Current Profile Dynamics in Tokamak Plasmas via the Minimal-Surface Theory

Chao Xu and Eugenio Schuster

***Abstract*— The central task of current profile control during the ramp-up phase of a tokamak discharge is to find the actuator trajectories that are necessary to achieve certain desired current profile at some time between the end of the ramp-up phase and early stage of the flattop phase. The magnetic diffusion partial differential equation (PDE) models the dynamics of the poloidal magnetic flux profile, which is closely related to the toroidal current density profile, and plays a key role in the model-based control synthesis. Given the initial and desired target profiles, splines are used in this work to generate evolutionary curves connecting their boundaries at both endpoints of the spatial domain. Then, a closed four-edge frame (initial profile, target profile, two boundary curves) in the three dimensional space (time, space, poloidal magnetic flux) is obtained without knowing the transient dynamics inside. The minimal surface theory is used in this work to define a surface spanned by the closed four-edge frame, which represents the desired transient dynamics for the poloidal magnetic flux. Then, the control task becomes a trajectory tracking problem. Once the desired transient dynamics is defined, the temporal and spatial derivatives of the poloidal magnetic flux in the magnetic diffusion equation can be computed, and the control-oriented PDE model can be reformulated into an algebraic equation where the control values at each time instant represent the to-be-determined unknown variables. Numerical simulation results show the effectiveness of this approach. This method is characterized by high speed computation and shows potential for real-time implementation in a closed-loop receding-horizon scheme, particularly for long-discharge tokamaks such as ITER.**

I. Introduction

Nuclear fusion is the process by which two nuclei fuse together to form a heavier nucleus. This process is accompanied by a release of energy, which is the result of the mass "lost" in the reaction. The amount of released energy is given by Einstein's famous equation (derived in 1905 as a part of his special theory of relativity), $E = (M_r - M_p)c^2$, where E is the energy, M_r the mass of the reactant nuclei, M_p the mass of the product nuclei, and c the speed of light. To make a fusion reaction possible, a certain amount of energy is required to bring two repellant nuclei carrying positive charges sufficiently close. To overcome the Coulomb barrier, the kinetic energy of the nuclei is increased by heating. The temperature required for a thermonuclear fusion reaction to take place is around 100 million degrees. At much lower temperatures (about 10 thousand degrees), the electrons and nuclei separate and create an ionized gas called plasma, also known as the fourth state of matter. The plasma conducts electricity and responds to magnetic fields, motivating a magnetic confinement approach to nuclear fusion. One type of magnetic confinement devices is the Tokamak, where a torus-shaped intangible bottle is created by magnetic fields to confine the high-temperature plasma.

This work was supported by the NSF CAREER award program (ECCS-0645086).

C. Xu (chx205@lehigh.edu) and E. Schuster are with the Department of Mechanical Engineering and Mechanics, Lehigh University, 19 Memorial Drive West, Bethlehem, PA 18015, USA.

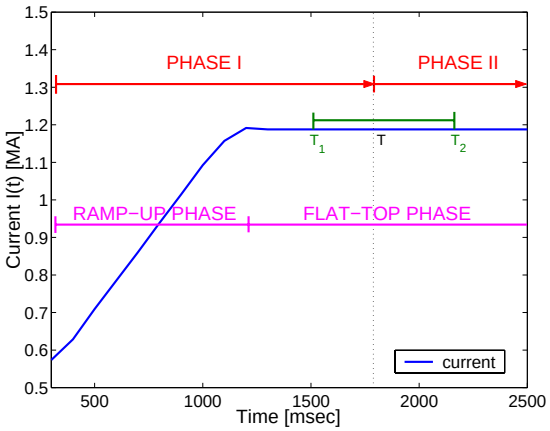

Fig. 1. The total plasma current evolution can be divided in several phases. In this work we focus on phase I, which includes the ramp-up phase and the first part of the flattop phase. The control goal is to drive the magnetic flux profile from some initial arbitrary profile to a predefined target profile at some time T within the time window $[T_1, T_2]$ in the flattop phase.

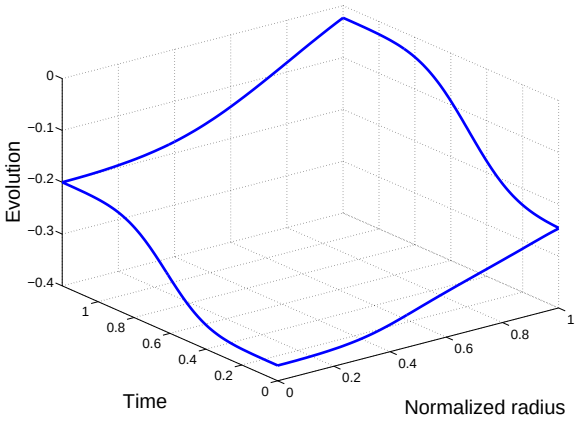

Fig. 2. The four-edge frame includes the initial magnetic flux distribution $\psi(\hat{\rho}, t_0)$ and the desired target magnetic flux distribution $\psi^{\mathrm{d}}(\hat{\rho})$ at the final time t_f. At the boundary $\hat{\rho} = 0$ and $\hat{\rho} = 1$, we connect $\psi_0(0)$ and $\psi^{\mathrm{d}}(0)$ to generate smooth transient dynamics for $\psi(0, t)$, and $\psi_0(1)$ and $\psi^{\mathrm{d}}(1)$ to generate smooth transient dynamics for $\psi(1, t)$.

During the ramp-up phase of a tokamak discharge (Fig. 1), multiple external sources (e.g., ohmic heating, neutral beam injection, radio frequency) can be used to control the spatial profile of many different plasma variables such as density, temperature, current, and rotation. Transport models usually governed by 1-D nonlinear coupled partial differential equations (PDEs) can be used to predict the plasma dynamics

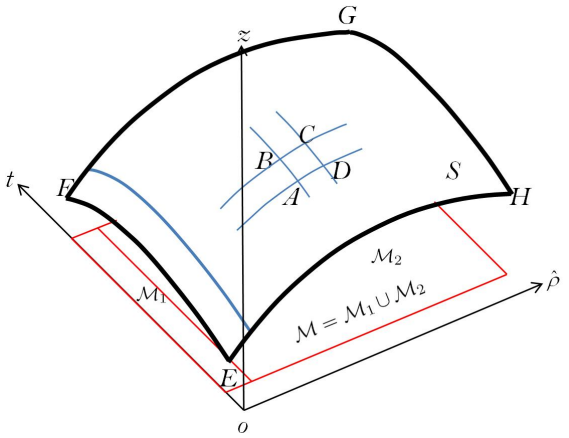

Fig. 3. Surface integral. The surface S over domain $\mathcal{M}$ is expressed by $z=\psi(\hat{\rho},t)$, $\forall(\hat{\rho},t)\in\mathcal{M}$. The coordinate of A is $(\hat{\rho}_0,t_0,z_0)$, where $z_0=\psi(\hat{\rho}_0,t_0)$. The coordinate of B is $(\hat{\rho}_0,t_0+dt,z_0+\psi_t(\hat{\rho}_0,t_0)dt))$, where $\psi_t(\hat{\rho}_0,t_0)=\frac{\partial\psi}{\partial t}(\hat{\rho}_0,t_0)$, and $d\hat{\rho}$ is the length of the line element $\overline{AB}$. The coordinate of D is $\big(\hat{\rho}_0+d\hat{\rho},t_0,z_0+\psi_{\hat{\rho}}(\hat{\rho}_0,t_0)d\hat{\rho})\big)$, where $\psi_{\hat{\rho}}(\hat{\rho}_0,t_0)=\frac{\partial\psi}{\partial\hat{\rho}}(\hat{\rho}_0,t_0)$, and $d\hat{\rho}$ is the length of the line element $\overline{AD}$. Then, the vector $\vec{AB}$ is $(0,dt,\psi_t(\hat{\rho}_0,t_0)dt)$ and the vector $\vec{AD}$ is $\big(d\hat{\rho},0,\psi_{\hat{\rho}}(\hat{\rho}_0,t_0)d\hat{\rho}\big)$. Therefore, the area of the element $\square ABCD$ is $\left|\vec{AB}\times\vec{AD}\right| = \left|(-\psi_{\hat{\rho}}(\hat{\rho}_0,t_0)dxdy,-\psi_t(\hat{\rho}_0,t_0)d\hat{\rho}dt,d\hat{\rho}dt)\right| = \sqrt{1+\psi^2_{\hat{\rho}}(\hat{\rho}_0,t_0)+\psi^2_t(\hat{\rho}_0,t_0)}d\hat{\rho}dt$.

with certain degree of accuracy (e.g., [1], [2]). Strong nonlinearities and model uncertainties add to the complexity of the problem. Different from the prediction problem, where inputs and initial profiles are given to calculate the time response, the control problem is to find admissible inputs that can drive the plasma from given initial profiles to the vicinity of predefined desired profiles. The solution of this problem is aimed at saving long trial-and-error periods of time currently spent by fusion experimentalists trying to manually adjust the time evolutions of the actuators to achieve the desired plasma profiles at some time during the early stage of the flattop phase.

We have recently proposed some advance nonlinear optimization techniques (e.g., extremum-seeking [3] and sequential quadratic programming [4]) to solve this very challenging problem, and we have used them for the control of the current profile evolution during the ramp-up phase of discharge in the DIII-D tokamak. Instead of solving the PDE-constrained optimization problem, which is often computationally costly, we can interpolate the transient dynamics by connecting the initial and desired final profiles. By choosing two feasible curves satisfying the spatial boundary conditions to connect the initial and desired final profiles at both boundary points, an optimal surface spanned by the four-edge frame (two boundary curves, initial and desired final profiles, see Fig. 2) can be obtained by solving a 2-D nonlinear elliptical PDE arising from the minimal surface theory in differential geometry (see, e.g., [5], [6]). This surface, which represents the desired transient dynamics, satisfies the boundary conditions and minimizes the dynamic fluctuations. Thus, the ramp-up-phase final-time optimal control problem becomes a trajectory tracking problem.

Knowing the desired temporal-spatial evolutions, both spatial and temporal derivatives of the distributed profiles can be computed. Thus, at each time instance the transport PDEs degenerate to algebraic equations at every spatial point where the control values are the only unknowns. Optimization problems can be formulated to solve the algebraic equations by taking into account the control constraints (see, e.g., [7], [8]). By using this proposed technique, the ramp-up current profile optimal control problem can be formulated into a least-square problem with algebraic constraints, which is much less computationally demanding.

The paper is organized as follows. The optimal control problem for the current profile system is introduced in Section II. The transient dynamics defined by the minimal surface theory is presented in Section III. In Section IV, algebraic equations for the unknown control values are formulated at each time instant and are later solved by the least square method. Simulation studies are presented in Section V. The paper is closed in Section VI by stating conclusions and future research remarks.

II. Statement of the Control Problem

A. Control-oriented model

To enable model-based control of the current profile at DIII-D, a control-oriented model for the dynamic evolution of the poloidal flux profile during and just following the ramp-up of the plasma current has been recently proposed [9]. During "Phase I" (see Fig. 1), mainly governed by the ramp-up phase, the plasma current is mostly driven by induction. In this case, it is possible to decouple the equation for the evolution of the poloidal flux $\psi(\hat{\rho},t)$ from the equation for the evolution of the temperature $T_e(\hat{\rho},t)$. The magnetic diffusion equation is combined with empirical correlations obtained at DIII-D for the temperature and non-inductive current to introduce a simplified dynamic model describing the evolution of the poloidal flux during the inductive phase of the discharge.

The current density j, that flows toroidally around the tokamak and whose profile must be controlled, is related to spatial derivatives of the poloidal magnetic flux ψ. We let ρ be an arbitrary coordinate indexing the magnetic surface. Any quantity constant on each magnetic surface could be chosen as the variable ρ. We choose the mean geometric radius of the magnetic surface as the variable ρ, i.e., $\pi B_{\phi,o}\rho^2=\Phi$, where $B_{\phi,o}$ is the reference toroidal magnetic field at the geometric plasma center R_o. The variable $\hat{\rho}$ denotes the normalized radius $\frac{\rho}{\rho_b}$, and ρ_b is the radius of last closed flux surface. The evolution of the poloidal flux in normalized cylindrical coordinates is given by the magnetic diffusion equation,

$$\frac{\partial\psi}{\partial t}=\frac{\eta(T_e)}{\mu_o\rho_b^2\hat{F}^2}\frac{1}{\hat{\rho}}\frac{\partial}{\partial\hat{\rho}}\left(\hat{\rho}\hat{F}\hat{G}\hat{H}\frac{\partial\psi}{\partial\hat{\rho}}\right)-R_o\hat{H}\eta(T_e)\frac{<\bar{j}_{NI}\cdot\bar{B}>}{B_{\phi,o}}, \tag{1}$$

where t is the time, ψ is the poloidal magnetic flux, η is the plasma resistivity, T_e is the plasma electron temperature, μ_o is the vacuum permeability, $\bar{j}_{NI}$ is the non-inductive source of current density (neutral beam, electron cyclotron, etc.), $\bar{B}$ is the toroidal magnetic field, and $<>$ denotes flux-surface

average. $\hat{F}, \hat{G}, \hat{H}$ are geometric factors, which are functions of $\hat{\rho}$. The boundary conditions of (1) are given by

$$\left.\frac{\partial \psi}{\partial \hat{\rho}}\right|_{\hat{\rho}=0}=0, \quad \left.\frac{\partial \psi}{\partial \hat{\rho}}\right|_{\hat{\rho}=1}=\frac{\mu_o}{2\pi}\frac{R_o}{\left.\hat{G}\right|_{\hat{\rho}=1}\left.\hat{H}\right|_{\hat{\rho}=1}}I(t), \quad (2)$$

where $I(t)$ denotes the total plasma current.

Highly simplified models for the temperature and non-inductive toroidal current density are chosen for the inductive phase of the discharge. Based on experimental observations at DIII-D, the shapes of the profiles are assumed to remain fixed and equal to the so-called reference profiles, which are identified from DIII-D discharges associated with the experiment of interest. The responses to the actuators are simply scalar multiples of the reference profiles.

The temperature T_e is assumed to follow

$$T_e(\hat{\rho},t)=k_{Te}T_e^{profile}(\hat{\rho})\frac{I(t)\sqrt{P}}{\bar{n}(t)}, \quad (3)$$

where the reference profile $T_e^{profile}$ is identified from DIII-D through Thomson scattering, and $k_{Te}=1.7295\cdot 10^{10}$ $\mathrm{m}^{-3}\mathrm{A}^{-1}\mathrm{W}^{-1/2}$. The average density $\bar{n}$ is defined as $\bar{n}(t)=\int_0^1 n(\hat{\rho},t)d\hat{\rho}$, where n denotes the plasma density.

The non-inductive toroidal current density $\frac{<\bar{j}_{NI}\cdot\bar{B}>}{B_{\phi,o}}$ is assumed to follow

$$\frac{<\bar{j}_{NI}\cdot\bar{B}>}{B_{\phi,o}}=k_{NIpar}j_{NIpar}^{profile}(\hat{\rho})\frac{I(t)^{1/2}P(t)^{5/4}}{\bar{n}(t)^{3/2}} \quad (4)$$

where the reference profile $j_{NIpar}^{profile}$ is identified from DIII-D through a combination of MSE diagnostics and the EFIT equilibrium reconstruction code, and $k_{NIpar}=1.2139\cdot 10^{18}$ $\mathrm{m}^{-9/2}\mathrm{A}^{-1/2}\mathrm{W}^{-5/4}$. The model for T_e and $\frac{<\bar{j}_{NI}\cdot\bar{B}>}{B_{\phi,o}}$ presented above considers neutral beams as the only source of current and heating. In the case where more heating and current sources are considered, equations (3) and (4) should include the weighted contributions of the different sources, and reference profiles need to be identified for each heating and current source. The resistivity η scales with the temperature T_e as $\eta(\hat{\rho},t)=\frac{k_{eff}Z_{eff}}{T_e^{3/2}(\hat{\rho},t)}$. where $Z_{eff}=1.5$, and $k_{eff}=4.2702\cdot 10^{-8}$ $\Omega\mathrm{m(keV)}^{3/2}$. By introducing

$$\vartheta_1(\hat{\rho})=\frac{k_{eff}Z_{eff}}{k_{Te}^{3/2}\mu_o\rho_b^2}\frac{1}{\hat{F}^2(\hat{\rho})(T_e^{profile}(\hat{\rho}))^{3/2}},\ D(\hat{\rho})=\hat{F}\hat{G}\hat{H},$$

$$\vartheta_2(\hat{\rho})=R_o\hat{H}\mu_o\rho_b^2\hat{F}^2(\hat{\rho})k_{NIpar}j_{NIpar}^{profile}(\hat{\rho}),\ k=\frac{\mu_o}{2\pi}\frac{R_o}{\hat{G}(1)\hat{H}(1)},$$

the normalized poloidal magnetic flux can be rewritten as

$$\frac{1}{\vartheta_1(\hat{\rho})}\frac{\partial\psi}{\partial t}=u_1(t)\frac{1}{\hat{\rho}}\frac{\partial}{\partial\hat{\rho}}\left[\hat{\rho}D(\hat{\rho})\frac{\partial\psi}{\partial\hat{\rho}}\right]-\vartheta_2(\hat{\rho})u_2(t). \quad (5)$$

The control inputs u_1 and u_2 are functions of physical actuators such as the total power P of the non-inductive current drive, the total plasma current I, and the average density $\bar{n}$, i.e.,

$$u_1(t)=\bar{n}^{1.5}I^{-1.5}P^{-0.75}, \quad u_2(t)=P^{0.5}I^{-1}. \quad (6)$$

The poloidal magnetic flux at the spatial boundaries is determined by the Neumann conditions

$$\frac{\partial\psi}{\partial\hat{\rho}}(0,t)=0, \quad \frac{\partial\psi}{\partial\hat{\rho}}(1,t)=ku_3(t), \quad u_3(t)=I. \quad (7)$$

where k is a constant. The initial condition for the magnetic flux profile is given by $\psi(\hat{\rho},t_0)=\psi_0(\hat{\rho})$.

B. Cost functional and constraints

In practice, the toroidal current density is usually specified indirectly by the rotational transform $\bar{\iota}$ (or the safety factor $q=\bar{\iota}^{-1}$), which is defined as $\bar{\iota}(\rho,t)=\frac{\partial\psi(\rho,t)}{\partial\Phi}$. The constant relationship between Φ and ρ, $\rho=\sqrt{\frac{\Phi}{\pi B_{\phi,o}}}$, and the definition of the normalized radius $\hat{\rho}$ allow us to rewrite the rational transform as $\bar{\iota}(\hat{\rho},t)=\frac{\partial\psi}{\partial\hat{\rho}}\frac{1}{B_{\phi,o}\rho_b^2\hat{\rho}}$. Since $\bar{\iota}$ is uniquely defined by the spatial derivative of the magnetic flux ψ, in this work we define the system output as $\iota(\hat{\rho},t)=\frac{\partial\psi}{\partial\hat{\rho}}$.

The control objective is to find control inputs $P(t)$ and $I(t)$ that minimize the cost functional

$$J=\frac{1}{2}\int_0^1\left|\iota(\hat{\rho},t_f)-\iota^{\mathrm{d}}(\hat{\rho})\right|^2d\hat{\rho}+\frac{1}{2}\int_{t_0}^{t_f}\left(\gamma_I I^2+\gamma_P P^2+\gamma_{\bar{n}}\bar{n}^2\right)dt,$$

where $\iota^{\mathrm{d}}(\hat{\rho})$ is the desired target profile at time t_f, and the positive constants γ_I, γ_P and $\gamma_{\bar{n}}$ are control weighting factors. The control actuators may need to satisfy constraints such as:

$$\text{Magnitude saturation: } \begin{pmatrix} I_l^{(0)}\le I\le I_u^{(0)}, \\ P_l\le P\le P_u \\ \bar{n}_l\le\bar{n}\le\bar{n}_u \end{pmatrix}; \quad (8)$$

$$\text{Rate saturation: } \left|\frac{dI(t)}{dt}\right|\le I_u^{(1)}; \quad (9)$$

$$\text{Initial and final values: } I(t_0)=I_0,\ I(t_f)=I_f. \quad (10)$$

III. Transient Dynamics Design

A. Edge design

By noting the definition $\iota(\hat{\rho},t)=\frac{\partial\psi}{\partial\hat{\rho}}$ for the system output, a desired target magnetic flux profile at the final time t_f, i.e. $\psi(\hat{\rho},t_f)=\psi^{\mathrm{d}}(\hat{\rho})$, can be obtained by integrating the desired output $\iota^{\mathrm{d}}(\hat{\rho})$ over $[0,\hat{\rho}]$, $(0\le\hat{\rho}\le 1)$:

$$\psi^{\mathrm{d}}(\hat{\rho})=\psi^{\mathrm{d}}(0)+\int_0^{\hat{\rho}}\iota^{\mathrm{d}}(\varrho)d\varrho=\psi^{\mathrm{d}}(1)-\int_{\hat{\rho}}^1\iota^{\mathrm{d}}(\varrho)d\varrho, \quad (11)$$

where either $\psi^{\mathrm{d}}(0)$ or $\psi^{\mathrm{d}}(1)$ need to be fixed to obtain the desired ψ^{d}-curve shown in Fig. 2. We can determine the left $(\psi(0,t_0)\ \ \psi(0,t_f))$ and right $(\psi(1,t_0),\ \psi(1,t_f))$ boundary values by using the compatibility conditions: $\psi(0,t_0)=\psi_0(0)$, $\psi(1,t_0)=\psi_0(1)$, $\psi(0,t_f)=\psi^{\mathrm{d}}(0)$ and $\psi(1,t_f)=\psi^{\mathrm{d}}(1)$. Thus, we add a sequence of points $\{\psi(0,T_i)\}_{i=1}^I, T_i\in(t_0,t_f)$, between $\psi(0,t_0)$ and $\psi(0,t_f)$, and a sequence of points $\{\psi(1,T_j)\}_{j=1}^J, T_j\in(t_0,t_f)$, between $\psi(1,t_0)$ and $\psi(1,t_f)$ to represent the left and right boundary evolution conditions (Dirichlet boundary conditions) via spline interpolations. Therefore, we obtain the four-edge frame shown in Fig. 2, where the surface within this frame representing the desired transient dynamics still needs to be defined.

B. Minimal surface

In Fig. 3, we define $\mathcal{M} = \{0 \le \hat{\rho} \le 1, t_0 \le t \le t_f\}$ in the $\hat{\rho}t$-plane with the boundary denoted by $\partial\mathcal{M}$. We define a three dimensional curve $\partial S \triangleq E \frown F \frown G \frown H \frown E$ over $\partial\mathcal{M}$, which can span a surface S in infinite many ways. In this work, the minimal surface theory is used to define a unique surface within the frame and minimize transient fluctuations. We discuss the detailed theory and algorithms in the rest of this subsection.

We use $z = \psi(\hat{\rho}, t)$ to express the surface S. As shown in Fig. 3, the minimal surface problem can be stated as the following optimization problem:

$$\min_{\psi(\hat{\rho},t)} \iint_M \sqrt{1 + \psi_{\hat{\rho}}^2(\hat{\rho},t) + \psi_t^2(\hat{\rho},t)}\, d\hat{\rho}dt, \tag{12}$$

subject to: $\psi(\hat{\rho}, t)|_{\partial\mathcal{M}} = g(\hat{\rho}, t) \triangleq$

$$\begin{cases} \psi_0(\hat{\rho}), & \hat{\rho} \in [0,1],\ t = t_0, \\ \text{Spline}\left(\psi(0,t_0), \{\psi(0,T_i)\}_{i=1}^{I}, \psi(0,t_f)\right), & T_i \in (t_0, t_f), \\ \text{Spline}\left(\psi(1,t_0), \{\psi(1,T_j)\}_{j=1}^{J}, \psi(1,t_f)\right), & T_j \in (t_0, t_f), \\ \psi^{\mathrm{d}}(\hat{\rho}), & \hat{\rho} \in [0,1],\ t = t_f, \end{cases}$$

where $\partial\mathcal{M}$ is the boundary of the domain $\mathcal{M}$. There are very few examples of minimal surfaces that can be expressed analytically. Nonlinear programming (NLP) can be used in general to find a numerical solution minimizing the area functional, but it is often computationally costly. Alternatively, by using the Euler-Lagrange equation in the calculus of variations [6], the minimal surface problem (12) can be reformulated as a nonlinear elliptic PDE:

$$\frac{\partial}{\partial\hat{\rho}}\left(\frac{\psi_{\hat{\rho}}}{\sqrt{1+\psi_{\hat{\rho}}^2+\psi_t^2}}\right) + \frac{\partial}{\partial t}\left(\frac{\psi_t}{\sqrt{1+\psi_{\hat{\rho}}^2+\psi_t^2}}\right) = 0,$$
$$\psi(\hat{\rho}, t)|_{\partial\mathcal{M}} = g(\hat{\rho}, t). \tag{13}$$

This is called the minimal-surface equation, which is impossible to solve analytically in general and numerical algorithms such as the finite element method (FEM) [10] or the finite difference method (FDM) [11] can be used to obtain numerical solutions.

One challenge arising during the implementation of the minimal surface theory for the definition of the transient dynamics of the magnetic flux is the satisfaction of the boundary conditions. In this problem, a Neumann boundary condition at $\hat{\rho} = 0$ must be satisfied. However, such spatial derivative requirement is not taken into account by the minimal surface equation (13). To overcome this challenge we decompose the domain into sub-domains and solve the minimal surface equation (nonlinear elliptic PDE) over each sub-domain with overlapping boundaries. In order to define a transient dynamics satisfying the zero Neumann boundary condition at $\hat{\rho} = 0$, we split the domain into two sub-domains $\mathcal{M} = \mathcal{M}_1 \cup \mathcal{M}_2$, where $\mathcal{M}_1$ is a narrow region of width $\bar{\Delta}\hat{\rho}$ along the $\hat{\rho} = 0$ boundary (Fig. 3). By properly defining Dirichlet boundary conditions for $\mathcal{M}_1$, it is possible to approximately satisfy the zero Neumann boundary condition at $\hat{\rho} = 0$.

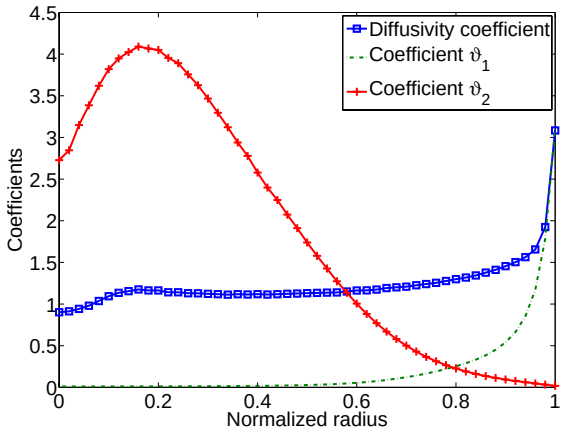

Fig. 4. Diffusivity coefficient D, coefficients $\vartheta_1(\times 10^{-15})$ and $\vartheta_2(\times 10^{13})$ versus the normalized radius $\hat{\rho}$.

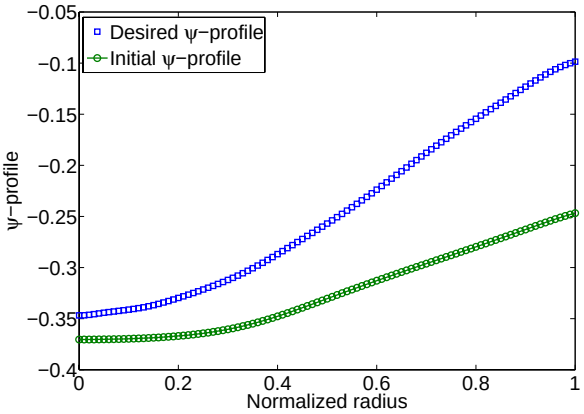

Fig. 5. The initial and desired profiles.

IV. Control Computations

A. Scalar analysis

In plasma discharge experiments at the DIII-D tokamak, the total power $P(t)$, the total plasma current $I(t)$, and the average density $\bar{n}(t)$ are of order 10^6W, 10^6A, and $10^{19}\mathrm{m}^{-3}$ respectively. The coefficients $\vartheta_1(\hat{\rho})$ and $\vartheta_2(\hat{\rho})$, which vary with respect to $\hat{\rho}$, are of order 10^{-15} and 10^{13}, respectively. The poloidal magnetic flux $\psi(\hat{\rho}, t)$, which varies with respect to both the normalized radius and time, is of order 10^{-1}. The other variables in (5) are of order 1. Thus, we can estimate the orders of all the terms in (5) and (6): $\frac{1}{\vartheta_1(\hat{\rho})}\frac{\partial\psi}{\partial t} \sim 10^{14}$, $u_1(t) \sim 10^{15}$, $u_1(t)\frac{1}{\hat{\rho}}\frac{\partial}{\partial\hat{\rho}}\left[\hat{\rho}D(\hat{\rho})\frac{\partial\psi}{\partial\hat{\rho}}\right] \sim 10^{14}$, $u_2(t) \sim 10^{-3}$ and $\vartheta_2(\hat{\rho})u_2(t) \sim 10^{10}$. Therefore, the interior control term $\vartheta_2(\hat{\rho})u_2(t)$ is small in comparison to other terms in (5).

B. Least square scheme

We consider a grid division $(\hat{\rho}_i, t_j)$ in the temporal-spatial domain $\mathcal{M} = \{0 \le \hat{\rho} \le 1, 0 \le t \le t_f\}$: $0 = \hat{\rho}_1 < \hat{\rho}_2 < \ldots < \hat{\rho}_i < \ldots < \hat{\rho}_M = 1$ and $t_0 = t_1 < t_2 < \ldots < t_j < \ldots < t_N = t_f$. We assume that the desired transient dynamics is obtained by solving the minimal surface equation (13) and is denoted by $\tilde{\psi}(\hat{\rho}, t)$ over $\mathcal{M}$. Then, we can compute the boundary control through

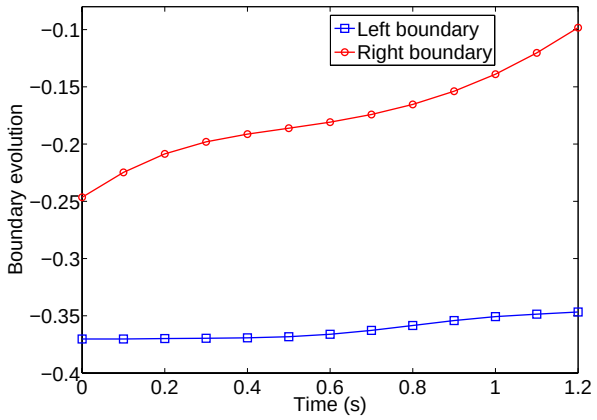

Fig. 6. The left and right profiles.

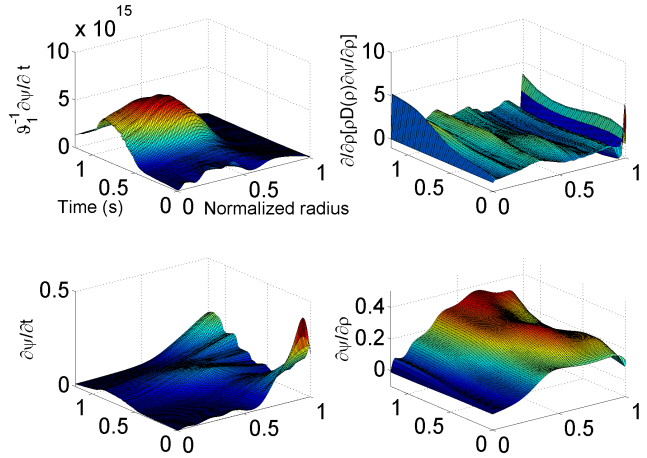

Fig. 7. Computational derivative.

the Neumann boundary condition (7), $u_3(t_n) = \frac{1}{k}\frac{\partial \tilde{\psi}}{\partial \hat{\rho}}(1, t_n)$, $n = 1, 2, \ldots, N$.

Based on the results of our order analysis, we let the interior control $u_2 = 10^{-3}$ and rewrite the PDE system (5) as the following linear system

$$\frac{1}{\hat{\rho}}\frac{\partial}{\partial \hat{\rho}}\left[\hat{\rho} D(\hat{\rho})\frac{\partial \psi}{\partial \hat{\rho}}\right] u_1(t) = \frac{1}{\vartheta_1(\hat{\rho})}\frac{\partial \psi}{\partial t} + \vartheta_2(\hat{\rho}) u_2(t), \quad (14)$$

where u_1 must be obtained at t_n, $n = 1, 2, \ldots, N$. For each t_n, $n = 1, 2, \ldots, N$, the equation (14) can be satisfied at each spatial node $\hat{\rho}_m$, $m = 2, 3, \ldots, M$, i.e.,

$$A^n_{2,M} u_1(t_n) = b^n_{2,M}, \quad n = 1, 2, \ldots, N, \quad (15)$$

where

$$A^n_{2,M} = \begin{pmatrix} \frac{1}{\hat{\rho}_2}\frac{\partial}{\partial \hat{\rho}}\left[\hat{\rho} D(\hat{\rho})\frac{\partial \tilde{\psi}(\hat{\rho}_2, t_n)}{\partial \hat{\rho}}\right] \\ \vdots \\ \frac{1}{\hat{\rho}_M}\frac{\partial}{\partial \hat{\rho}}\left[\hat{\rho} D(\hat{\rho})\frac{\partial \tilde{\psi}(\hat{\rho}_M, t_n)}{\partial \hat{\rho}}\right] \end{pmatrix}, \quad (16)$$

$$b^n_{2,M} = \begin{pmatrix} \frac{1}{\vartheta_1(\hat{\rho}_2)}\frac{\partial \tilde{\psi}(\hat{\rho}_2, t_n)}{\partial t} + \vartheta_2(\hat{\rho}_2) u_2(t_n) \\ \vdots \\ \frac{1}{\vartheta_1(\hat{\rho}_M)}\frac{\partial \tilde{\psi}(\hat{\rho}_M, t_n)}{\partial t} + \vartheta_2(\hat{\rho}_M) u_2(t_n) \end{pmatrix}. \quad (17)$$

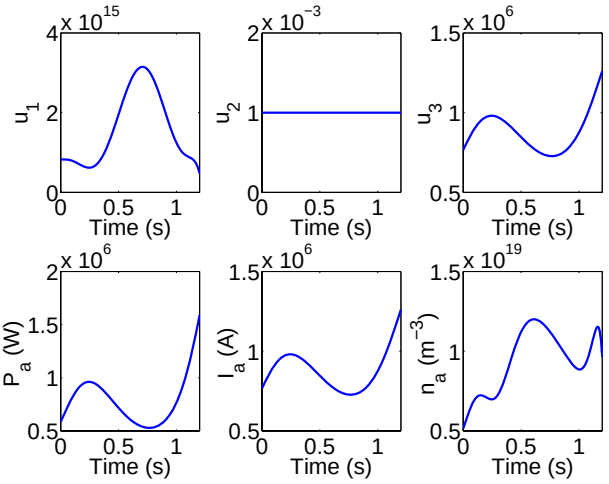

Fig. 8. Computed control functions.

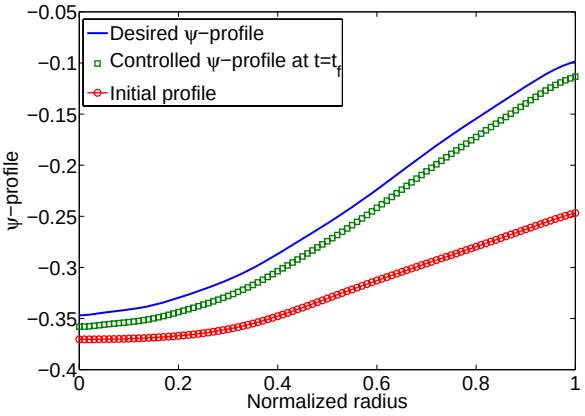

Fig. 9. Controlled ψ profile.

Without considering any actuation constraint, we can obtain the least square solution of the linear system (15) as

$$u^n_1 = u_1(t_n) = \left\{\left[A^n_{2,M}\right]^T A^n_{2,M}\right\}^{-1}\left[A^n_{2,M}\right]^T b^n_{2,M}. \quad (18)$$

In general, we can formulate the following optimization problem in the presence of actuation constraints:

$$\min_{\mathbf{u}_1 \in \mathcal{U}} \frac{1}{2}\beta_1 \|\mathbf{u}_1\|^2 + \frac{1}{2}\sum_{n=1}^{N} \beta_{2,n} \left\|A^n_{2,M} u_1(t_n) - b^n_{2,M}\right\|^2,$$

where $\mathbf{u}_1 = (u_1(t_1), \ldots, u_1(t_n), \ldots, u_1(t_f))^T$, β_1 and $\beta_{2,n}$ are positive weighting constants and $\mathcal{U}$ is the admissible control set defined by (8)-(10) at $t = t_n$, $n = 1, 2, \ldots, N$. This is a quadratic programming problem which can be solved relatively fast.

C. Computational derivatives

The matrices in (15) include both the temporal and spatial derivatives of the desired transient dynamics $\tilde{\psi}(\hat{\rho}, t)$ over $\mathcal{M}_{m,n} = (\hat{\rho}_m, t_n)$, $m = 1, 2, \ldots, M$ and $n = 1, 2, \ldots, N$. Using the discrete values $\tilde{\psi}(\hat{\rho}_{m-1}, t_n)$, $\tilde{\psi}(\hat{\rho}_m, t_n)$ and $\tilde{\psi}(\hat{\rho}_{m+1}, t_n)$ defined on a uniform grid, we can obtain the

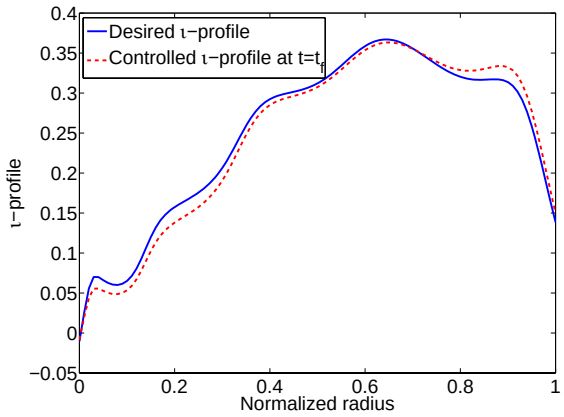

Fig. 10. Controlled ι profile.

spatial second-order difference formulas:

$$\frac{\partial\tilde{\psi}}{\partial\hat{\rho}}(\hat{\rho}_1,t_n)\approx\frac{-3\tilde{\psi}(\hat{\rho}_1,t_n)+4\tilde{\psi}(\hat{\rho}_2,t_n)-\tilde{\psi}(\hat{\rho}_3,t_n)}{2\Delta\hat{\rho}},$$
$$\frac{\partial\tilde{\psi}}{\partial\hat{\rho}}(\hat{\rho}_m,t_n)\approx\frac{\tilde{\psi}(\hat{\rho}_{m+1},t_n)-\tilde{\psi}(\hat{\rho}_m,t_n)}{2\Delta\hat{\rho}},\quad m\in[2,M-1],$$
$$\frac{\partial\tilde{\psi}}{\partial\hat{\rho}}(\hat{\rho}_M,t_n)\approx\frac{\tilde{\psi}(\hat{\rho}_{M-2},t_n)-4\tilde{\psi}(\hat{\rho}_{M-1},t_n)+3\tilde{\psi}(\hat{\rho}_M,t_n)}{2\Delta\hat{\rho}},$$

where $\Delta\hat{\rho}$ is the spatial step length. The term $\frac{1}{\hat{\rho}}\frac{\partial}{\partial\hat{\rho}}\left[\hat{\rho}D(\hat{\rho})\frac{\partial\tilde{\psi}(\hat{\rho}_m,t_n)}{\partial\hat{\rho}}\right]$ is computed using similar second-order difference formulas in terms of the previously obtained $\frac{\partial\tilde{\psi}(\hat{\rho}_m,t_n)}{\partial\hat{\rho}}$ for $m=1,2,\ldots,M$. The temporal difference formulas are obtained following identical procedure.

V. Numerical Example

The geometrical parameters $D(\hat{\rho})$, $\vartheta_1(\hat{\rho})$ and $\vartheta_2(\hat{\rho})$ in model (5) are shown in Fig. 4. The initial and desired profiles of the magnetic flux $\psi(\hat{\rho},t)$ are given in Fig. 5. We use splines to define the boundary evolutions over $\partial\mathcal{M}$, which are shown in Fig. 6. Then, we generate a triangular grid division over the domain $\mathcal{M}=\mathcal{M}_1\cup\mathcal{M}_2$. We solve the minimal surface equation (13) over the discrete nodes in both $\mathcal{M}_1$ and $\mathcal{M}_2$ using the finite element method.

In order to formulate the linear algebraic equation (15), we compute every term in (5) in terms of both the temporal and spatial derivatives, which are shown in Fig. 7. We obtain the control functions shown in Fig. 8 where we let $u_2(t)=10^{-3}$. Thus, we can obtain the physical actuators (denoted by P_a, I_a and n_a) taking into account the definitions (6) and (7). Using the obtained actuator functions, we simulate the PDE system (5) with boundary conditions (6). The obtained control functions can drive the system to the vicinity of the desired profile with a similar shape of the desired profile. This is illustrated in Fig. 9, where desired and actual flux profiles are compared. The error at the final time t_f seems to be rather constant with respect to space, which implies that the desired shape for the ι profile is achieved. Fig. 10 compares the desired ι profile with the actual ι profile at time t_f. The rather constant flux error may be used to redefine $\psi^{\mathrm{d}}(0)$ (or $\psi^{\mathrm{d}}(1)$) during the definition of the desired magnetic flux target profile.

VI. Conclusion

The open-loop finite-time optimal current profile control problem arising in tokamak plasmas during the ramp-up phase of the discharge is solved by using the minimal surface theory and the least square method (or the quadratic programming method when actuation constraints are taken into account). The minimal surface theory is used to generate the desired transient dynamics and then a tracking problem can be formulated for the current profile control. Knowing the transient dynamics, every term containing both temporal and spatial derivatives in the control-oriented PDE model can be computed using the finite difference method. Thus, the control-oriented PDE model becomes a set of algebraic equations where the only unknowns are the control functions at different instants of time.

Taking into account the control constraints, these algebraic equations can be reformulated as a quadratic programming problem. When no actuator constraint needs to be taken into account, the quadratic programming problem simplifies to a simple least square problem. Numerical studies demonstrate that this approach can significantly reduce computational effort, showing potential for real-time implementation in a closed-loop receding-horizon scheme, particularly for long-discharge tokamaks such as ITER.

Simulation results show that the numerical optimization procedure can generate control trajectories driving the final ψ-profile to the proximity of a predefined desired profile. Future work includes the implementation of this method directly in terms of the ι variable in order to eliminate relatively spatially-constant matching errors that can appear in the ψ variable, which are indeed not important. Alternatively, an iterative scheme can be designed where the matching error is used to redefine the desired magnetic flux target profile, and therefore the transient dynamics, for the following iteration.

References

[1] F. Hinton and R. Hazeltine, "Theory of plasma transport in toroidal confinement systems," *Reviews of Modern Physics*, vol. 48, no. 2, pp. 239–308, 1976.

[2] J. Blum, *Numerical Simulation and Optimal Control in Plasma Physics*. New York: John Wiley &. Sons, 1988.

[3] Y. Ou, C. Xu, E. Schuster, T. Luce, J. Ferron, and M. Walker, "Extremum-seeking open-loop control of plasma current profile at the DIII-D tokamak," *Plasma Phys. Control. Fusion*, vol. 50, p. 115001 (24pp), 2008.

[4] C. Xu, J. Dalessio, Y. Ou, and E. Schuster, "Pod-based optimal control of current profile in tokamak plasmas via nonlinear programming," *Proceedings of the 2008 American Control Conference*, 2008.

[5] R. Courant, *Dirichlet's Principle, Conformal Mapping, and Minimal Surfaces*. New York: Interscience Publishers, Inc., 1950.

[6] R. Courant and D. Hilbert, *Methods of Mathematical Physics*. New York: Interscience Publishers, Inc., 1953.

[7] S. Boyd and L. Vandenberghe, *Convex Optimization*. New York: Cambridge University Press, 2004.

[8] J. Nocedal and S. Wright, *Numerical Optimization (2nd edition)*. New York: Springer, 2006.

[9] Y. Ou *et al.*, "Towards model-based current profile control at DIII-D," *Fusion Engineering and Design*, vol. 82, pp. 1153–1160, 2007.

[10] P. Ciarlet, *The Finite Element Method for Elliptic Problems*. New York: North-Holland, 1979.

[11] W. Schiesser, *The Numerical Method of Lines*. New York: Academic Press, 1991.